

Original Article

A micellized bone morphogenetic protein-7 prodrug ameliorates liver fibrosis by suppressing transforming growth factor- β signaling

Kyungjoo Cho^{1,2*}, Nam Hee Kim^{3*}, Sang Hyun Seo^{1,2}, Sang Hyun Song³, Chul Hee Jeong³, Hyun Sil Kim³, Jo Eun Um⁴, Minhee Ku^{6,7}, Jaemoon Yang^{6,7}, Jun Yong Park^{1,2,5}, Sang Hoon Ahn^{2,5}, Jong In Yook^{3,4}, Seung Up Kim^{1,2,5}

¹Brain Korea 21 PLUS Project for Medical Science, Yonsei University College of Medicine, Seoul, Korea; ²Yonsei Liver Center, Severance Hospital, Seoul, Korea; ³Department of Oral Pathology, Oral Cancer Research Institute, Yonsei University College of Dentistry, Seoul, Korea; ⁴MET Life Sciences Ltd, Seoul, Korea; ⁵Department of Internal Medicine, Institute of Gastroenterology, Yonsei University College of Medicine, Seoul, Korea; ⁶Department of Radiology, Yonsei University College of Medicine, Seoul, Korea; ⁷Convergence Research Center for Systems Molecular Radiological Science, Yonsei University, Seoul, Korea. *Equal contributors.

Received November 23, 2021; Accepted January 7, 2022; Epub February 15, 2022; Published February 28, 2022

Abstract: Bone morphogenetic protein-7 (BMP-7) antagonizes transforming growth factor- β (TGF- β), which is critically involved in liver fibrogenesis. Here, we designed a micelle formulation consisting of a protein transduction domain (PTD) fused BMP-7 polypeptide (mPTD-BMP-7) to enhance endocytic delivery, and investigated its ability to ameliorate liver fibrosis. The mPTD-BMP-7 formulation was efficiently delivered into cells via endocytosis, where it inhibited TGF- β mediated epithelial-mesenchymal transition. After successfully demonstrating delivery of fluorescently labeled mPTD-BMP-7 into the murine liver in vivo, we tested the mPTD-BMP-7 formulation in a murine liver fibrosis model, developed by repeated intraperitoneal injection of hepatotoxic carbon tetrachloride, twice weekly from 4 to 16 weeks. mPTD-BMP-7 effects were tested by injecting the mPTD-BMP-7 formulation (or vehicle control) into the lateral tail at a dose of 50 (n=8) or 500 μ g/kg (n=10), also twice per week from 4 to 16 weeks. Vehicle-treated control mice developed fibrous septa surrounding the liver parenchyma and marked portal-to-portal bridging with occasional nodules, whereas mice treated with mPTD-BMP-7 showed only fibrous expansion of some portal areas, with or without short fibrous septa. Using the Ishak scoring system, we found that the fibrotic burden was significantly lower in mPTD-BMP-7 treated mice than in control mice (all $P < 0.001$). Treatment with mPTD-BMP-7 protected tight junctions between hepatocytes and reduced extracellular matrix protein levels. It also significantly decreased mRNA levels of collagen 1A, smooth muscle α -actin, and connective tissue growth factor compared with that in control mice (all $P < 0.001$). Collectively, our results indicate that mPTD-BMP-7, a prodrug formulation of BMP-7, ameliorates liver fibrosis by suppressing the TGF- β signaling pathway in a murine liver fibrosis model.

Keywords: Bone morphogenetic protein, trans-activator of transcription-fusion polypeptide, liver fibrosis, transforming growth factor

Introduction

Persistent hepatocyte death and compensatory regeneration caused by chronic hepatic injury promotes liver fibrosis, characterized by extracellular matrix remodeling and excessive collagen deposition [1]. Without appropriate treatment, chronic liver injury ultimately progresses to advanced liver fibrosis or cirrhosis, which are major risk factors for hepatocellular carcinoma, a disease that affects millions of patients worldwide [2-4].

The activation of quiescent hepatic stellate cells (HSCs), initiated by paracrine signaling from damaged hepatocytes and activated Kupffer cells, is considered the pivotal pathogenic event in liver fibrosis [5, 6]. Activated HSCs produce fibrillar collagens and overexpress α -smooth muscle actin (α -SMA), matrix metalloproteinase (MMP)-2, and MMP-9, all of which cause accumulation of fibrotic extracellular matrix [7]. HSC activation is mediated by various cytokines, including transforming growth factor- β (TGF- β), tumor necrosis factor- α ,

and platelet-derived growth factor [8]. Of these, TGF- β is strongly involved in liver fibrogenesis, as well as induction of apoptosis, oxidative stress and differentiation of HSCs into hepatocytes [6].

In contrast to TGF- β , bone morphogenetic proteins (BMPs) participate in anti-fibrogenic processes [9]. Among BMP subtypes, BMP-7 induces ectopic bone and cartilage formation, and plays a crucial role in renal development [10]. Thus, most information regarding the role of BMP-7 has come from renal fibrosis studies [11], which have demonstrated that BMP-7 exerts a protective, anti-fibrotic effect by antagonizing TGF- β -induced epithelial-mesenchymal transition (EMT). A recent study showed that adenovirus-mediated ectopic expression of BMP-7 reduced expression levels of α -SMA, type I collagen and hydroxyproline in a thioacetamide-induced liver fibrosis model [12]. Furthermore, ectopic expression of BMP-7 in mice promotes parenchymal cell proliferation, which particularly impacts hepatocytes [13].

On the basis of these data, researchers have used recombinant BMPs for regenerative therapy in both animal studies and human clinical trials [14]. However, the performance of BMPs in further studies has been limited by the rapid clearance and enzymatic degradation of recombinant BMPs. To overcome intrinsic limitations that affect the fate of such exogenously introduced soluble factors in cells, we developed a recombinant BMP-7 polypeptide that exploits endogenous protein processing to produce active BMP-7 from a prodrug formulation. Specifically, we created a construct in which cationic human immunodeficiency virus-derived trans-acting transcriptional activator (TAT), a membrane-permeant peptide used as a protein transduction domain (PTD) to transduce the protein into cells, was linked to a furin-mediated protein cleavage site, allowing secretion of latent BMP-7 with a prodomain [15].

Although PTD-mediated protein transduction represents an attractive pharmacological strategy, limitations of cargo size and endosomal escape have restricted its therapeutic application [16, 17]. In this study, we designed a micelle formulation of PTD-BMP-7 (mPTD-BMP-7) to enhance endosomal transduction in cells and hepatic delivery in vivo. We also investigated whether mPTD-BMP-7 polypeptide-a

prodrug type of BMP7 that exploits the PTD technique for post-translational processing and secretion of active BMP-7-ameliorates liver fibrosis by suppressing the TGF- β signaling pathway in cultured HSCs in-vitro and in a mouse model of carbon tetrachloride (CCl₄)-induced liver fibrosis.

Methods

Cell culture and transfection

LX2 primary human HSCs were obtained from the Seo research group [18] and maintained at 37°C in a humidified atmosphere with 5% CO₂. 293A cells were provided by H.W. Park (Yonsei University, Seoul, Korea). 293A and LX2 cells were cultured in Dulbecco's modified Eagle's medium (DMEM; Gibco, Grand Island, NY, USA) supplemented with 10% fetal bovine serum (Gibco) and 1 \times penicillin-streptomycin (Welgene, Gyeongsan, Korea). Mouse hepatocyte NCTC 1469 cells were obtained from the Korean Cell Line Bank and maintained in DMEM with 10% horse serum. The specified amount of recombinant protein was directly applied to serum-free culture medium. For 3TP-lux reporter activity, LX2 cells were transiently transfected with 100 ng of 3TP-lux reporter vector (11767, Addgene, Watertown, USA) and 1 ng of SV40 Renill expression vector (Promega, WI, USA, E6911) using Lipofectamine 2000 (11668-019, Invitrogen, Waltham, MA, USA). The combination of 1 ng recombinant human TGF- β (240-B, R&D systems, Minneapolis, MN, USA), mPTD-BMP-7, geldamycin and KNK437 were treated into cells. Geldanamycin and KNK437 were purchased from CAYMAN. Cells were lysed at 24 h after treatment and the relative ratio of renilla luciferase to firefly luciferase activity was measured in a dual luciferase assay (Promega, Madison, WI, USA, E1910). Recombinant human Noggin (120-10C) was purchased from PEPPROTECH (NJ, USA).

Immunoblotting and immunofluorescence analysis of cells

For the western blot analyses, protein extracts were prepared in Triton X-100 lysis buffer (50 mM Tris pH 7.4, 150 mM NaCl, 1 mM EDTA, 1% triton X-100). The antibodies against pSMAD 1/5/8 (13820s) and SMAD1 (9743s) were purchased from Cell signaling (Danvers, MA, USA).

Bone morphogenetic protein-7 ameliorates liver fibrosis

Total SMAD1 served as a loading control. For immunofluorescence analysis, the cells were treated with mPTD-BMP-7 and recombinant noggin for 1 h and washed twice with ice-cold PBS and incubated for 15 min at room temperature with 3% formaldehyde in PBS. The cells were permeabilized with 0.5% Triton X-100 for 5 min and then blocked for 1 h in PBS containing 3% bovine serum albumin followed by incubation with Xpress (R910-25, Invitrogen), pSMAD1/5/8 (13820s, Cell signaling, Danvers, MA, USA), and YAP (sc-101199, Santa Cruz, CA, US) primary antibody overnight at 4°C. Cells were then washed three times with PBS containing 0.1% Tween 20 followed by incubation with anti-mouse-Alexa Fluor-488 (for green, A11008, Invitrogen) or anti-rabbit-Alexa Fluor-594 (for red, A11005, Invitrogen) secondary antibody. Cellular fluorescence was monitored using confocal microscopy (Zeiss LSM780).

mPTD-BMP-7 preparation

The bacterial expression vectors for Xpress-tagged PTD-BMP-7 and protein purification were described previously [15]. The denatured polypeptide was micellized with filtered 0.1% egg lecithin (BOC Sciences, Shirley, NY, USA) by means of sonication. For in vivo fluorescent imaging, PTD-BMP-7 or human recombinant BMP-2 was labeled with indocyanine green (ICG-sulfo-O Su, Dojindo Molecular Technologies, Rockville, MD, USA). For immunofluorescence analysis, PTD-BMP-7 was labeled using an Alexa Fluor 488 protein labeling kit (Invitrogen). PTD-BMP-7 was stained with 5% uranyl acetate for transmission electron microscopy (TEM). For cellular transduction, mPTD-BMP-7 was directly added to the culture medium. The mPTD-BMP-7 particle size was routinely determined by direct light scattering (ELSZ-200ZS, Otsuka Electronics, Osaka, Japan). The prepared mPTD-BMP-7 formulation was analyzed using a field emission scanning electron microscope (Merlin, Zeiss, Oberkochen, Germany).

Animals

All experiments involving live mice were performed in accordance with the Guidelines and Regulations for the Care and Use of Laboratory Animals in AAALAC-accredited facilities. The study protocol was approved by the Animal

Policy and Welfare Committee of the Yonsei University College of Medicine (Permit number: 2018-0088). The mice used were 4-week-old C57BL/6 males purchased from Orientbio Inc. (Seongnam, Korea).

For in vivo distribution analysis, BALB/c nude mice were administered 10 µg of indocyanine green-labeled mPTD-BMP-7 via the tail vein and subjected to in vivo fluorescent imaging at each time point. Fluorescence images were acquired by VISQUE® InVivo Smart (Vieworks, Anyang, Korea) and analyzed by CleVue™ software (Vieworks). Total signal intensity ($\{[p/s/cm^2/sr]/[\mu W/cm^2]\} \cdot cm^2$) was normalized by subtraction of control (vehicle) signal intensity. After 6 h, the mice were sacrificed and major organs were harvested for ex vivo fluorescence imaging and histological analysis.

CCl₄ and mPTD-BMP-7 treatment

CCl₄ was administered to mice twice weekly at a dose of 1 ml/kg body weight [19]. Mice were monitored regularly following the administration of CCl₄, and treated and sacrificed in accordance with institutional guidelines. Either vehicle or the mPTD-BMP-7 formulation was injected into the lateral tail vein of the mice, twice per week from 4 to 16 weeks, at a dose of 50 µg/kg (low-dose group, n=8) or 500 µg/kg (high-dose group, n=10). All mice in the control group received an equal volume of vehicle through the tail vein following the same treatment schedule. The mice were monitored regularly following the administration of CCl₄ and mPTD-BMP-7, and were treated and sacrificed in accordance with institutional guidelines.

Serum biochemical assays, liver harvest, and tissue processing

Mice were deeply anesthetized by intraperitoneal injection of tiletamine/zolazepam (Zoletil™, 30 mg/kg) and xylazine (10 mg/kg). A mid-line laparotomy incision was then performed and the maximum possible amount of blood was collected from the inferior vena cava. Pieces of extracted liver were immersed in freshly prepared 10% neutral-buffered formalin and incubated overnight. The remainder of the liver was snap-frozen in liquid nitrogen and stored at -70°C until subsequent use. Serum samples were harvested following centrifugation of clotted blood. Aspartate amino-

Bone morphogenetic protein-7 ameliorates liver fibrosis

Table 1. Sequences of quantitative real-time PCR primers

Genes	Forward primer sequence (5'→3')	Reverse primer sequence (5'→3')
hSnail	TCT CTG AGG CCA AGG ATC TC	CTT CGG ATG TGC ATC TTG AG
hVimentin	AAT GGC TCG TCA CCT TCG TGA AT	CAG ATT AGT TTC CCT CAG GTT CAG
hE-cadherin	TGA GTG TCC CCC GGT ATC CTC	CAG TAT CAG CCG CTT TCA GAT TTT
hOccludin	CGG TCT AGG ACG CAG CAG AT	AAG AGG CCT GGA TGA CAT GG
hGAPDH	TCC GCG GCT ATA TGA AAA CAG	TCG TAG TGG GCT TGC TGA A
CTGF	AGA ACT GTG TAC GGA GCG TG	GTG CAC CAT CTT TGG CAG TG
Col1A1	TGG GAT TCC CTG GAC CTA A	GCT CCA GCT TCT CCA TCT TT
α-SMA	TCA GGG AGT AAT GGT TGG AAT G	GGT GAT GAT GCC GTG TTC TA
E-cadherin	GAG ACC AGT TTC CTC GTC CG	GAG CAG CTC TGG GTT GGA TT
Vimentin	CTT GAA CGG AAA GTG GAA TCC T	GTC AGG CTT GGA AAC GTC C
Fibronectin	TCA GAA GAG TGA GCC CCT GA	GGA AGG GTA ACC AGT TGG GG

transferase (AST) and alanine aminotransferase (ALT) levels were examined using an automated clinical chemistry analyzer (Dri-Chem 4000i; Fujifilm, Tokyo, Japan).

Histological assessment of liver fibrosis

Liver specimens embedded in paraffin blocks were sectioned into 4- μ m slices. The slices were stained with Masson's trichrome stain and Picrosirius red in accordance with standard protocols. Slides were analyzed and photographed using an inverted microscope (Eclipse Ti; Nikon, Tokyo, Japan) equipped with a digital camera. Histological grading of liver fibrosis was performed using Ishak's score [20]. Fields from each slide were randomly selected and analyzed for Picrosirius red-positive areas using ImageJ (NIH, Bethesda, MD, USA).

Immunohistochemistry and immunofluorescence analysis of mouse tissue

Paraffin sections were deparaffinized in xylene and rehydrated by ethanol gradient. The antigen epitopes were then unmasked using sodium citrate buffer (pH, 6.0). Subsequently, sections were incubated overnight at 4°C using the anti-Xpress (Invitrogen) and anti-activated caspase-3 (Cell Signaling Technology, Danvers, MA, USA) primary antibodies. Sections were then incubated with the appropriate biotinylated secondary antibodies, followed by treatment with freshly prepared DAB substrates (Vector Laboratories, Burlingame, CA, USA). Sections were lightly counterstained with hematoxylin and mounted. For assessment of apoptosis, activated caspase-3-positive cells were counted in liver sections after visualization using a

microscope (Eclipse Ti; Nikon) at 200 \times magnification. For immunofluorescence, sections were prepared and hydrated; they were then boiled with citrate (pH=6.0), permeabilized in PBS supplemented with 0.2% Triton X-100, and blocked with 10% normal donkey serum (Jackson ImmunoResearch, West Grove, PA, USA) for 1 h at room temperature. Sections were subsequently incubated overnight with primary antibodies at 4°C. After they had been washed with PBS, the sections were incubated with secondary antibodies, stained with DAPI, and embedded using Fluoromount-G (Invitrogen). Fluorescence images were obtained using a Zeiss LSM 780 confocal microscope (Carl Zeiss, Jena, Germany).

RNA purification, reverse transcription, and real-time polymerase chain reaction amplification

The isolation of total RNA from extracted livers (TRIzol; Invitrogen) and synthesis of first-strand cDNA (Superscript III Synthesis Kit; Invitrogen) were performed in accordance with the manufacturer's protocols. A PCR master mix (Power SYBR Green PCR Master Mix; Applied Biosystems, Foster City, CA, USA) was used for quantitative PCR with the StepOnePlus™ PCR System (Applied Biosystems). Relative expression levels of target genes were normalized to the levels of GAPDH. The sequences of real-time PCR primers used in this study are shown in **Table 1**.

Statistical analysis

Statistical analyses were conducted using unpaired Student's t-tests. Significant differ-

ences between the two groups are denoted by asterisks (* $P < 0.05$, ** $P < 0.01$, and *** $P < 0.001$).

Results

Technical strategy and endosomal transduction of mPTD-BMP-7 into cells

To overcome the limitation of cargo size associated with PTD-fusion polypeptides, we designed the nanocarrier, mPTD-BMP-7 (**Figure 1A**). The typical micelle size, as determined by direct light scattering, was ~180-200 nm. Scanning electron microscopy demonstrated that mPTD-BMP-7 was actively transduced into cells and was successfully dispersed into the Golgi apparatus (**Figure 1B**). An analysis of z-stacks obtained by laser-scanning confocal following direct addition of mPTD-BMP-7 clearly showed mPTD-BMP-7 in the cytosolic space, confirming intracellular delivery (**Figure 1C**). To further examine endosomal delivery, we transfected cells with endosomal markers (Rab5 or Rab7 GTPases) and treated them with fluorescently labeled mPTD-BMP-7. We found that mPTD-BMP-7 co-localized with Rab5 or Rab7 (**Figure 1D**), indicating that mPTD-BMP-7 was delivered into cells via endosomal pathways. To directly observe intracellular transduction, we added uranyl acetate-stained mPTD-BMP-7 to 293A cells and examined cells by transmission electron microscopy, which showed that mPTD-BMP-7 was entrapped by membrane vesicles at 1 h and was actively transported into the cytosolic space at 6 h (**Figure 1E**).

Endosomal mPTD-BMP-7 antagonizes TGF- β -mediated EMT via SMAD1/5/8 activation

The broad-spectrum therapeutic potency of BMP-7 reflects counteraction of TGF- β signaling through SMAD1/5/8 activation [9, 21]. To determine whether mPTD-BMP-7 elicits SMAD1/5/8 activation, we exposed 293A cells and the HSC cell line LX2 to mPTD-BMP-7 and examined levels of the activated (phosphorylated) form of SMAD1/5/8 (pSMAD1/5/8). mPTD-BMP-7 induced an increase in pSMAD1/5/8 levels that peaked at 30 min and was sustained up to 60 min (**Figure 2A**). Furthermore, Noggin specifically sequesters active BMP-7 [22], we examined SMAD1/5/8 activation after adding mPTD-BMP-7 with Noggin. The results showed that mPTD-BMP did not

effect on pSMAD1/5/8 abundance and nuclear translocation in the presence of Noggin (**Figure 2A** and **2B**). Treatment with different concentrations of mPTD-BMP-7 for 30 min induced a concentration-dependent increase in pSMAD1/5/8 levels (**Figure 2C**). This analysis showed that mPTD-BMP-7 acts through activation of SMAD1/5/8 to suppress TGF- β signaling. The endosomal transduction of mPTD-BMP-7, described above, suggests that the denatured PTD-BMP-7 polypeptide is renatured by heat shock proteins (HSPs)-molecular chaperones that participate in protein maturation and refolding [23]. To test this hypothesis, we measured the effects of mPTD-BMP-7 on TGF- β activity by co-treating 293A cells with TGF- β and mPTD-BMP-7 and measuring the abundance of mRNA for *SERPINE1*, a direct transcriptional target of TGF- β , in the presence of geldanamycin, a specific inhibitor of HSP90, or KNK437, an inhibitor of HSP105, HSP72, and HSP40 (**Figure 2D**). In 293A cells co-treated with TGF- β and mPTD-BMP-7, geldanamycin failed to prevent mPTD-BMP-7 inhibition of TGF- β signaling, as evidenced by the complete absence of TGF- β -induced *SERPINE1* expression. In contrast, KNK437 blocked mPTD-BMP-7-mediated inhibition of TGF- β , resulting in sustained expression of *SERPINE1* (**Figure 2D**). Collectively, these results suggest that mPTD-BMP-7 is renatured by HSPs other than HSP90. Because TGF- β is a well-known inducer of EMT [24], we examined EMT markers in TGF- β -treated LX2 cells co-treated with mPTD-BMP-7. We found that mPTD-BMP-7 reversed TGF- β -mediated EMT by reducing transcripts levels of snail and vimentin and enhancing transcripts level of E-cadherin and occludin (**Figure 2E**). During TGF- β -mediated EMT, the transcriptional co-activator YAP1 (Yes-associated protein) is translocated to the nucleus, where it acts on its downstream target CTGF (connective tissue growth factor) to play a critical role in tissue fibrosis [25-27]. To examine the effects of mPTD-BMP-7 on EMT, we treated 293A cells with TGF- β in the presence or absence of mPTD-BMP-7 and evaluated YAP1 activation by assessing its nuclear localization. TGF- β treatment significantly enhanced YAP1 nuclear translocation, an effect that was strongly attenuated by mPTD-BMP-7 treatment (**Figure 2F**). These results indicate that mPTD-BMP-7 efficiently blocks TGF- β -mediated EMT through a YAP1-CTGF axis. We next examined

Bone morphogenetic protein-7 ameliorates liver fibrosis

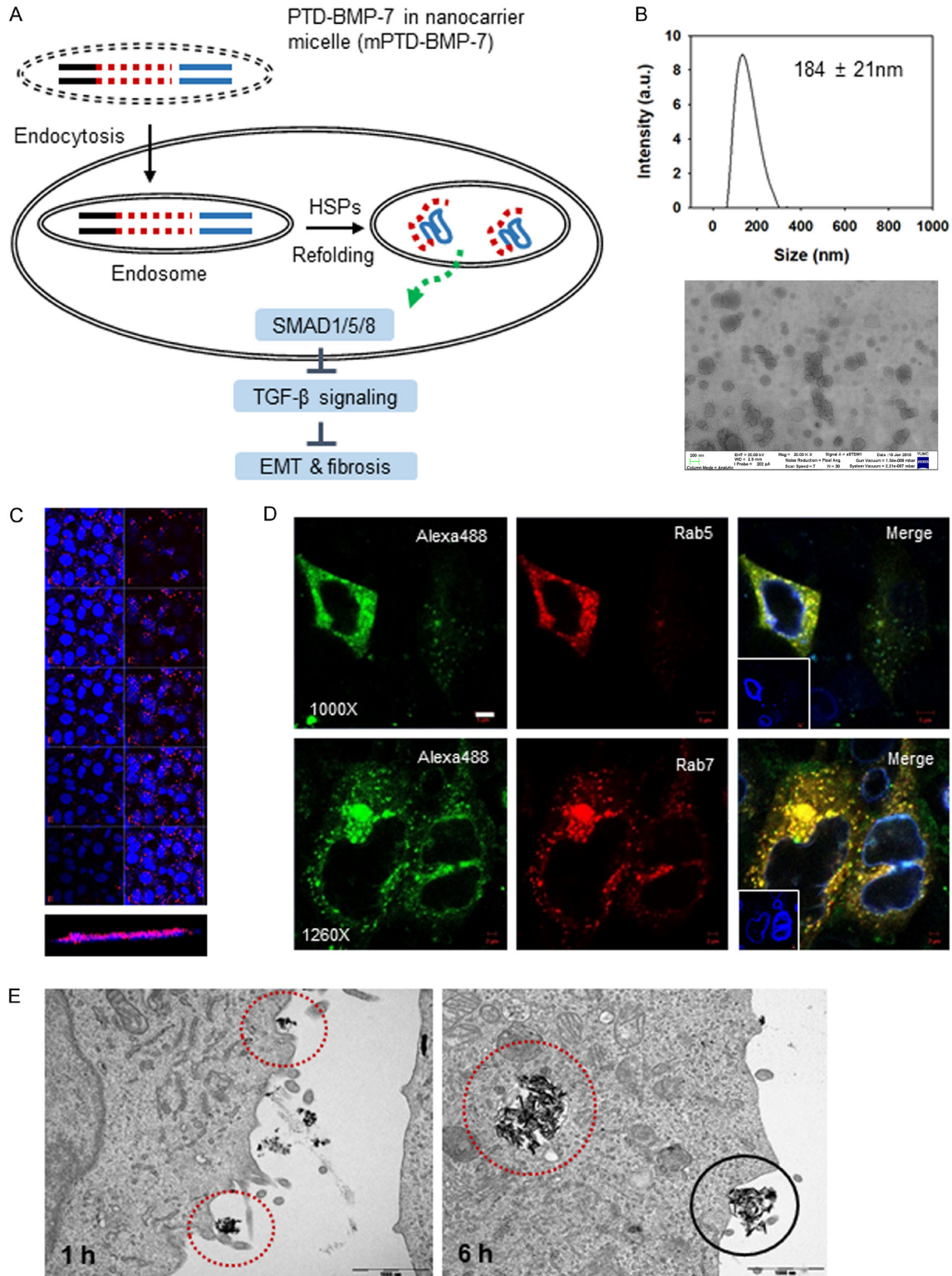


Figure 1. Schematic diagram of the technical strategy and preparation of nanocarrier micelle BMP-7 (mPTD-BMP-7) for endosomal transduction into target cells. **A.** Schematic diagram of the use of pro-drug BMP-7 to counteract TGF- β signaling. **B.** Direct light scattering and scanning electron microscope images of mPTD-BMP-7 revealing nano-sized particles. Scale bar, 200 nm. **C.** 293A cells were treated with 100 ng mPTD-BMP-7 for 8 h and confocal images were taken. Lower panel represents the Z-stack section of confocal images. **D.** 293A cells were transiently transfected with the endosomal markers, mCherry-fused Rab5 or Rab7, and treated with Alexa-488 labeled mPTD-BMP-7 for 16 h

Bone morphogenetic protein-7 ameliorates liver fibrosis

h. Scale bar, 4 μ m. E. Uranyl acetate-stained PTD-BMP-7 prepared in micelles were added to 293A cells, which were subjected to transmission electron microscopy. Red dotted circles denote stained PTD-BMP-7. Note the continuous endosomal uptake into target cells (black circle). Scale bar, 1,000 nm.

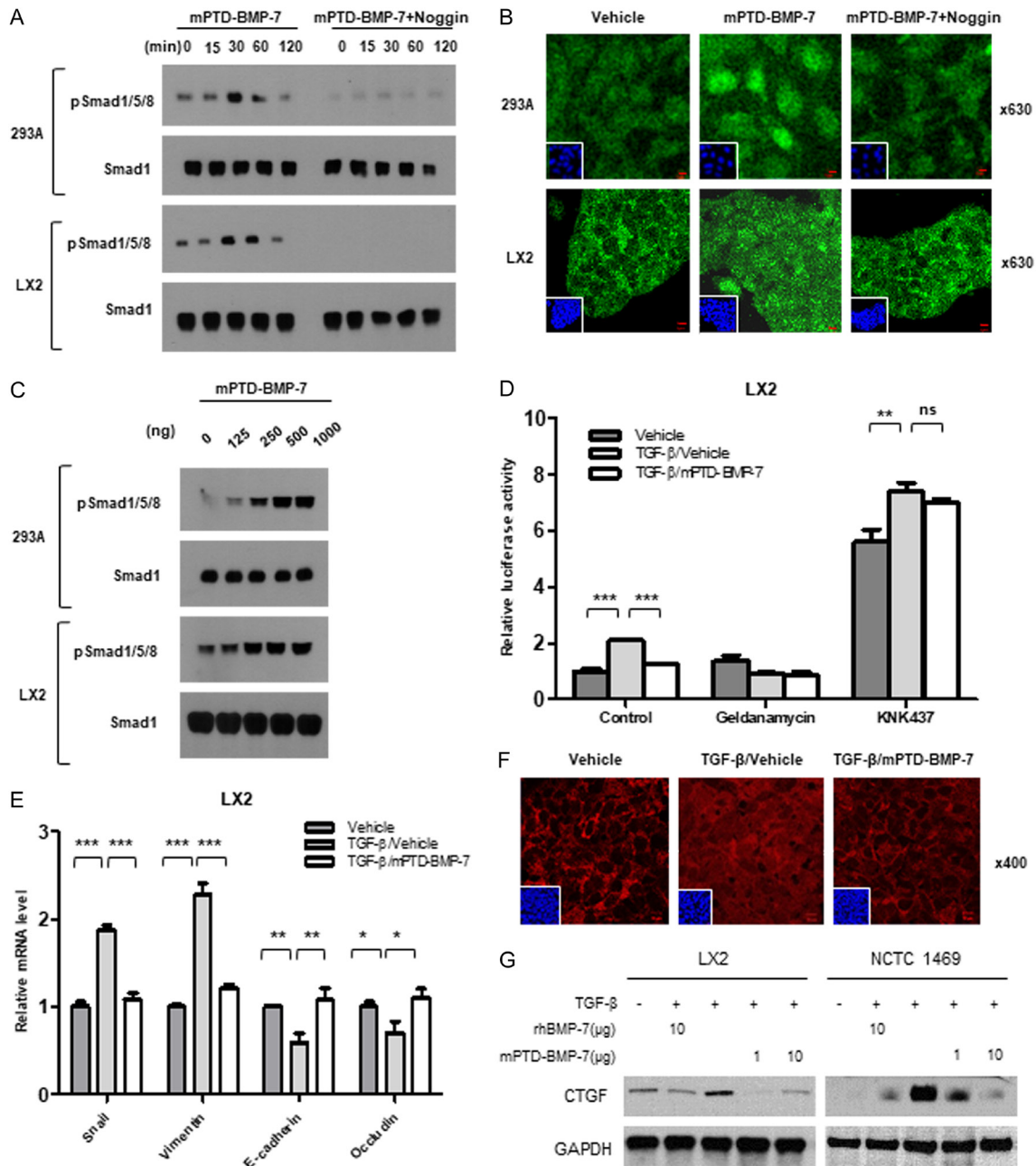


Figure 2. Endosomal mPTD-BMP7 antagonizes TGF- β -mediated EMT via SMAD1/5/8 activation. **A.** 293A and HSC LX2 cells were treated with mPTD-BMP-7 (500 ng) in the present or absence of recombinant Noggin (1 μ g) for the indicated times. Levels of p-SMAD1/5/8 and SMAD1 were determined by immunoblotting analysis. Total SMAD1 served as a loading control. **B.** 293A and HSC LX2 cells were treated with 500 ng of mPTD-BMP-7 for 1 h and phospho-SMAD1/5/8 nuclear translocation was examined by confocal microscopy. Scale bar, 5 μ m. **C.** 293A and HSC LX2 cells were treated with various concentrations of mPTD-BMP-7 as indicated for 1 h and cell lysates were subjected to immunoblotting analysis of p-SMAD1/5/8. Total SMAD1 served as a loading control. **D.** HSC LX2 cells were transiently transfected with the TGF- β -responsive reporters 3TP-Lux, and treated with HSP inhibitors (Geldanamycin 20 μ M and KNK437 50 μ M) for 16 h. Luciferase activity in cells treated with TGF- β and mPTD-BMP-7 was analyzed using the dual luciferase assay system. The 3TP-lux transactivation values were normalized to the activity of a

Bone morphogenetic protein-7 ameliorates liver fibrosis

co-transfected SV40-Renilla construct. Relative fold changes were compared to control vehicle group (error bars, \pm SD. n.s., not significant, * $P < 0.05$, ** $P < 0.01$, and *** $P < 0.001$ compared with vehicle). E. LX2 cells were treated with TGF- β (1 ng) in combination with mPTD-BMP-7 for 24 h and relative transcript levels of EMT marker (Snail, Vimentin, E-cadherin, and Occludin) were determined by qPCR-PCR (error bars, \pm SD., * $P < 0.05$, ** $P < 0.01$, and *** $P < 0.001$). F. Confluent 293A cells were treated with TGF- β (5 ng) in combination with vehicle or mPTD-BMP-7 (100 ng) under serum-free conditions, and intracellular Yes-associated protein localization or CTGF transcript abundance was detected by immunofluorescence. Scale bar, 10 μ m. G. HSC LX2 and mouse hepatocyte NCTC 1469 cells were treated with TGF- β (5 ng) in combination with recombinant human BMP-7 or mPTD-BMP-7 for 48 h, and CTGF abundance was determined by immunoblotting analysis. GAPDH served as a loading control.

whether mPTD-BMP-7 also inhibits TGF- β activation in HSCs and hepatocytes by examining CTGF expression in LX2 and NCTC 1469 cells, respectively, following treatment with TGF- β in combination with recombinant human BMP-7 or mPTD-BMP-7. We found that both mPTD-BMP-7 and recombinant human BMP-7 blocked TGF- β -mediated CTGF expression in LX2 and NCTC 1469 cells (**Figure 2G**).

Intravenously administered mPTD-BMP-7 is mainly distributed to the liver and is transduced into hepatocytes

Nano-sized particles in the bloodstream are mainly sequestered in the liver and spleen [28]. Because mPTD-BMP-7 is a nanoparticle formulation, we presumed that intravenously administered mPTD-BMP-7 would be delivered to the liver. To test this hypothesis, we covalently conjugated indocyanine green to mPTD-BMP-7 and administered this compound to mice via the tail vein. An in vivo fluorescence analysis showed that mPTD-BMP-7 mainly accumulated in the ventral side of the abdominal space (**Figure 3A**), suggesting that mPTD-BMP-7 is efficiently detected in the liver. After 6 h, mPTD-BMP-7 was mainly delivered to the liver (~95%), whereas lower amounts of mPTD-BMP-7 were found in the spleen (<3%), lungs (<1%), and kidneys (<1%). No fluorescence signals were detected in the brain, skin, or muscle (**Figure 3B**). Hematoxylin and eosin-staining and immunohistochemical analyses of liver tissue harvested 16 h after administration of mPTD-BMP-7 showed that mPTD-BMP-7 was successfully delivered into hepatocytes, especially in portal veins (**Figure 3C**).

Effects of mPTD-BMP-7 on gross liver morphology and liver enzymes

To investigate the therapeutic effects of the mPTD-BMP-7 prodrug on liver fibrosis, we tested it in a liver fibrosis model developed by repeated intraperitoneal injection of mice with

hepatotoxic CCl₄, twice per week from 4 to 16 weeks (**Figure 4A**). Mice were administered mPTD-BMP-7 at doses of 50 μ g/kg (low-dose group, n=8) or 500 μ g/kg (high-dose group, n=10), also twice weekly from 4 to 16 weeks. At sacrifice (16 weeks), gross liver size and ratio of liver weight to body weight decreased in mice treated with a low or high dose of mPTD-BMP-7 compared with that in vehicle controls (n=10; $P < 0.05$) (**Figure 4B**). Serum aspartate aminotransferase (AST) and alanine aminotransferase (ALT) levels, indicative of liver injury, were significantly lower in mPTD-BMP-7-treated mice than control mice (all $P < 0.001$) (**Figure 4C**). These results indicate that treatment with mPTD-BMP-7 might be beneficial for preventing liver injury due to exposure to hepatotoxins.

Histopathological characterization of mPTD-BMP-7 effects

Histological examinations with Masson's trichrome and Picrosirius red staining were used to visualize the extent of fibrotic changes. Masson's trichrome staining clearly revealed fibrous septa surrounding the liver parenchyma and marked portal-to-portal bridging with occasional nodules in the vehicle control group, whereas samples from mPTD-BMP-7-treated groups showed only fibrous expansion of some portal areas, with or without short fibrous septa (**Figure 5A**, left). Ishak scoring analysis revealed that the fibrotic burden was significantly lower in mPTD-BMP-7-treated mice than in control mice (all $P < 0.001$) (**Figure 5A**, right). Similar findings were observed after Picrosirius red staining: collagen bands were less noticeable in both low- and high-dose mPTD-BMP-7-treated groups showed mice than in control mice (**Figure 5B**, left). Morphometric measurement of collagen fibers based on Picrosirius red staining confirmed that liver fibrosis was significantly reduced in mPTD-BMP-7-treated mice compared with control mice, and that this effect was dose-dependent (**Figure 5B**, right).

Bone morphogenetic protein-7 ameliorates liver fibrosis

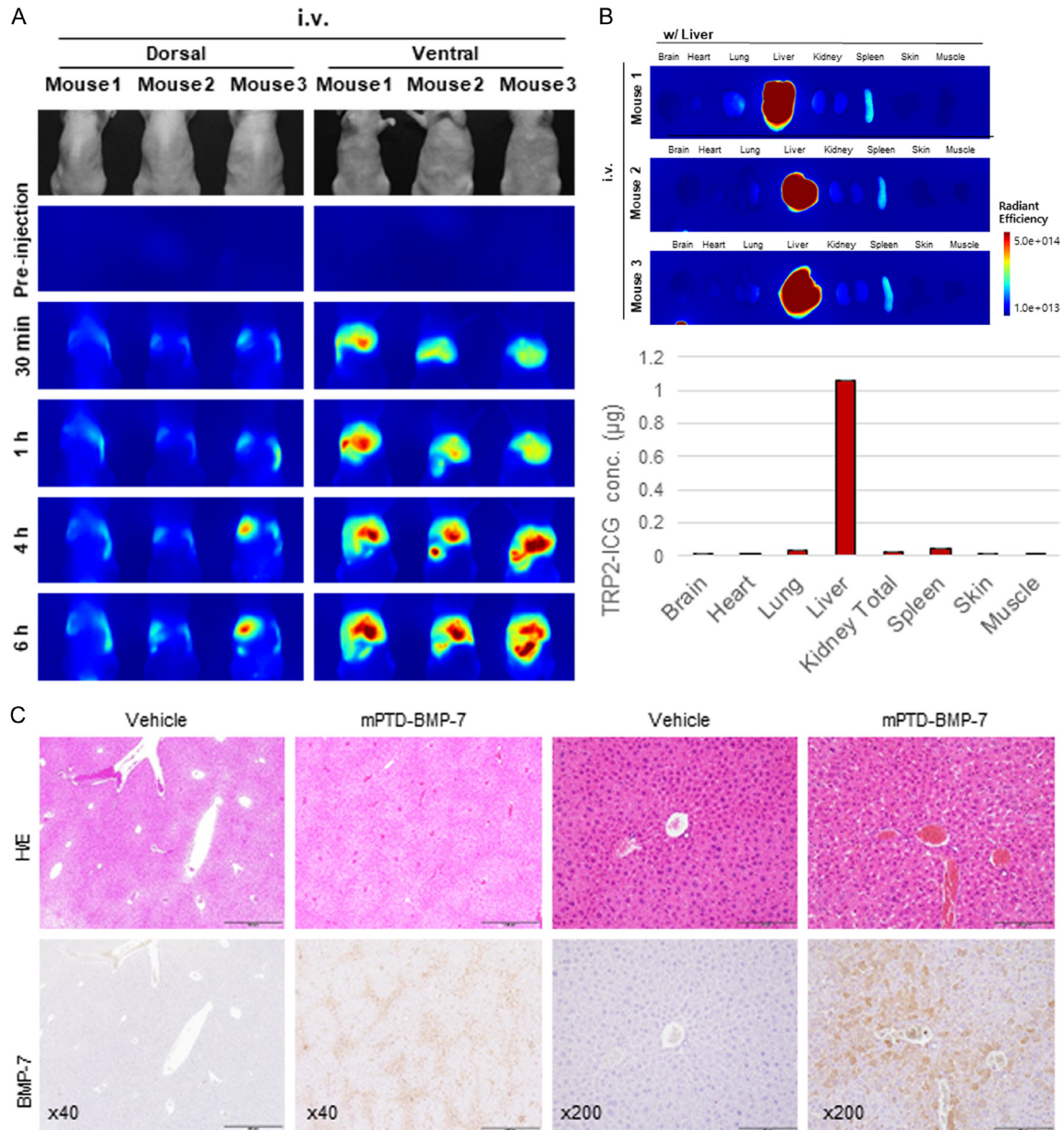


Figure 3. Intravenously administered mPTD-BMP7 is mainly delivered to the liver and transduced into hepatocytes. A. Ten micrograms of indocyanine green-labeled mPTD-BMP-7 were injected via mouse tail vein, and the biodistribution of mPTD-BMP-7 was assessed by in vivo fluorescence imaging. B. After 6 h of intravenous injection, the major organs of mice were dissected and ex vivo fluorescence images were taken (upper) for quantitative analysis (lower). C. Ten micrograms of mPTD-BMP-7 were administered via mouse tail vein, and the livers were harvested at 16 h after injection for hematoxylin and eosin staining (upper) and Xpress tag immunohistochemistry (lower). Scale bar, 500 µm for 40×, 200 µm for 200×.

Expression levels of the tight junction protein, ZO-1, were significantly higher in mPTD-BMP-7-treated mice than in control mice (**Figure 5C**). Collectively, these results indicate that mPTD-BMP-7 interrupts fibrogenesis and protects tight junctions between hepatocytes during liver injury.

Effects of mPTD-BMP-7 on cell apoptosis, fibrogenic signaling, and EMT

Increased hepatocyte apoptosis and necrosis are commonly observed in fibrotic livers [29]. To investigate the effects of mPTD-BMP-7 on apoptosis, we performed immunohistochemi-

Bone morphogenetic protein-7 ameliorates liver fibrosis

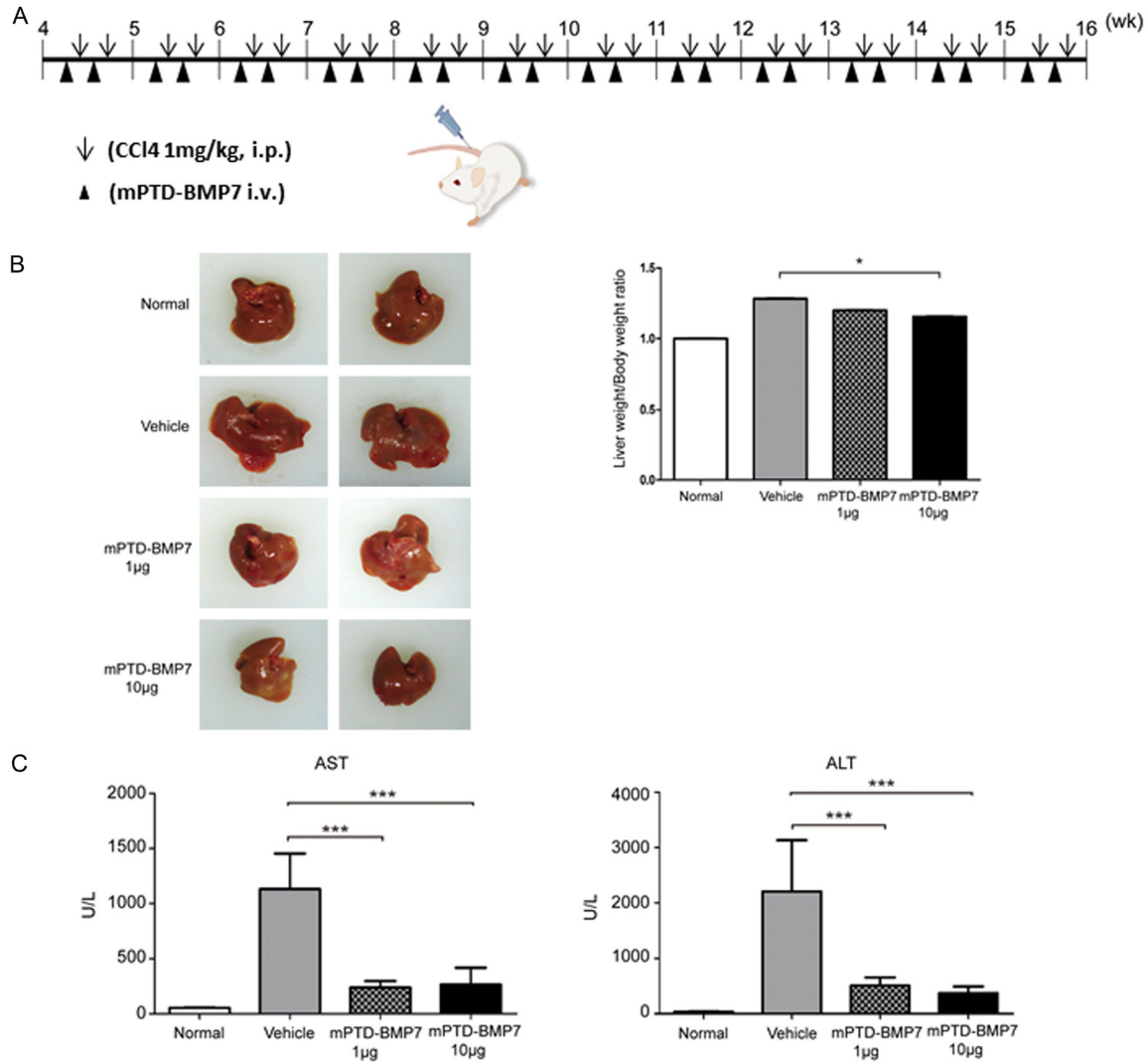


Figure 4. Effects of mPTD-BMP-7 on gross morphology and liver enzymes. A. Experimental schematic of the establishment of the mouse liver fibrosis model. Liver fibrosis was induced by intraperitoneal injection of carbon tetrachloride (CCl₄; 1 ml/kg body weight) twice weekly. Mice in the mPTD-BMP-7 + CCl₄ group received tail vein injections of mPTD-BMP-7 (1 and 10 µg) twice per week, beginning with administration of CCl₄. B. Gross morphology and liver weight/body weight ratios of livers harvested from mice in each group at 3 months post-injection. C. Aspartate aminotransferase and alanine aminotransferase activities.

cal staining for cleaved caspase-3 as a surrogate marker of apoptosis. Significantly lower levels of hepatocyte apoptosis were observed in mPTD-BMP-7-treated mice than in control mice ($P < 0.001$, **Figure 6A**). Furthermore, the pro-inflammatory cytokine, interleukin-1 β , and pro-apoptotic gene, Bax, were downregulated in mPTD-BMP-7-treated livers (**Figure 6B**). An investigation of cellular mechanisms underlying fibrogenesis showed that expression levels of α -SMA and CTGF-major markers of activated HSCs-were significantly reduced in livers of mPTD-BMP-7-treated mice at both mRNA and

protein levels (**Figure 6C** and **6D**). In contrast, levels of epithelial markers, including ZO-1, were elevated in livers of mPTD-BMP-7-treated mice (**Figure 6C**). mRNA expression levels of vimentin and fibronectin, markers of mesenchymal cells, and collagen, a marker of liver fibrosis, were significantly suppressed in livers of mPTD-BMP-7-treated mice ($P < 0.05$) (**Figure 6D**). Collectively, these results indicate that mPTD-BMP-7 suppresses the accumulation of extracellular matrix components, activation of HSCs, and induction of fibrogenic processes in the liver.

Bone morphogenetic protein-7 ameliorates liver fibrosis

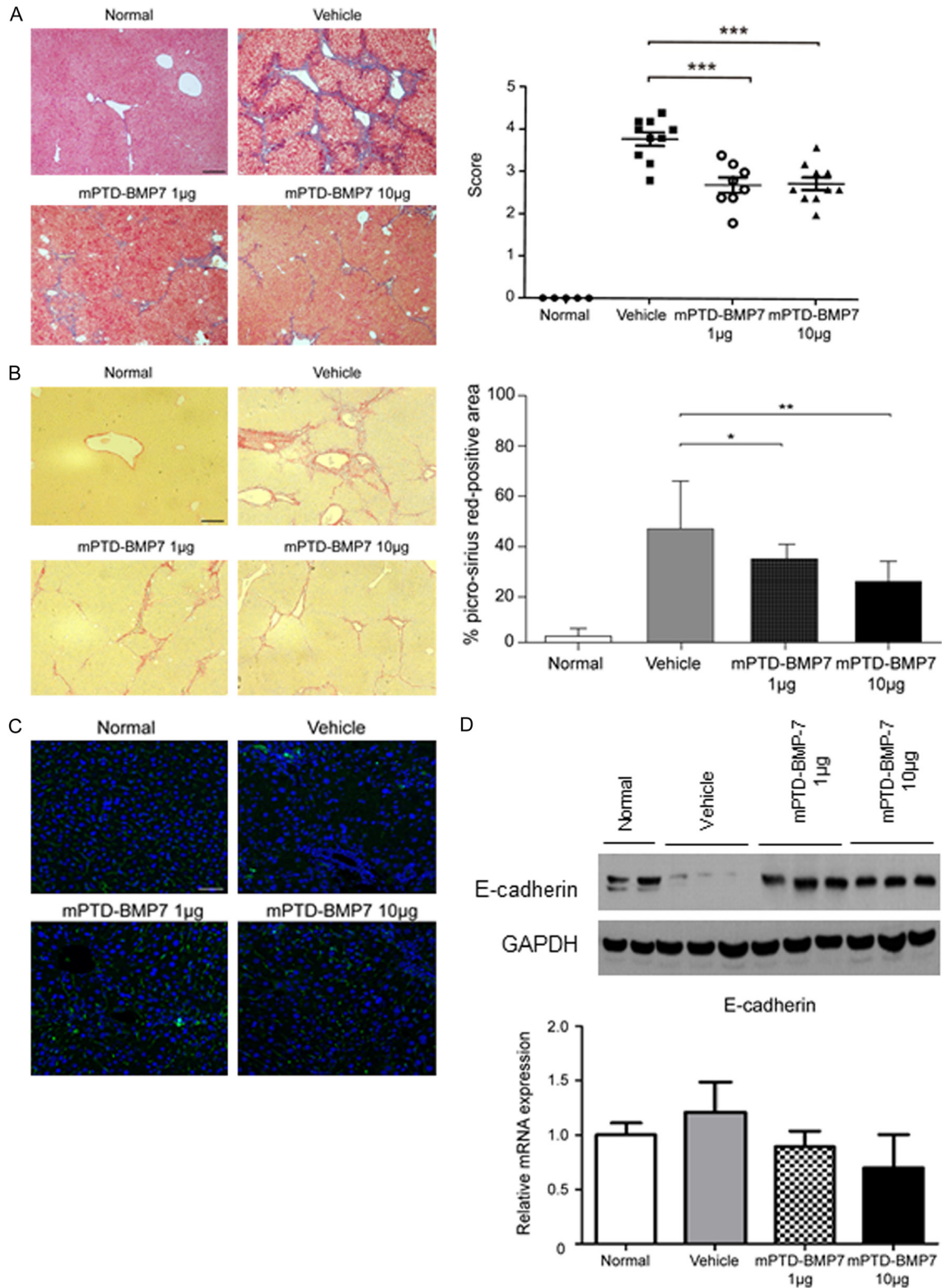


Figure 5. Effects of mPTD-BMP-7 on histopathological characteristics. A. Masson's trichrome staining was used to detect accumulated collagen in liver sections from vehicle, CCl₄, and CCl₄ + mPTD-BMP-7 groups at 12 weeks. Scale bars, 100 µm (left). Fibrotic burden was graded using the Ishak scoring system (right). B. Images of picrosirius red staining. Scale bars, 100 µm (left). The Picrosirius red-positive area was quantified using ImageJ (right). C. Immunofluorescence staining for ZO-1 on liver sections from mice treated with vehicle, CCl₄, or CCl₄ + mPTD-BMP-7 for 12 weeks. Scale bars, 50 µm. D. Protein and gene expression levels of E-cadherin in the indicated groups.

Bone morphogenetic protein-7 ameliorates liver fibrosis

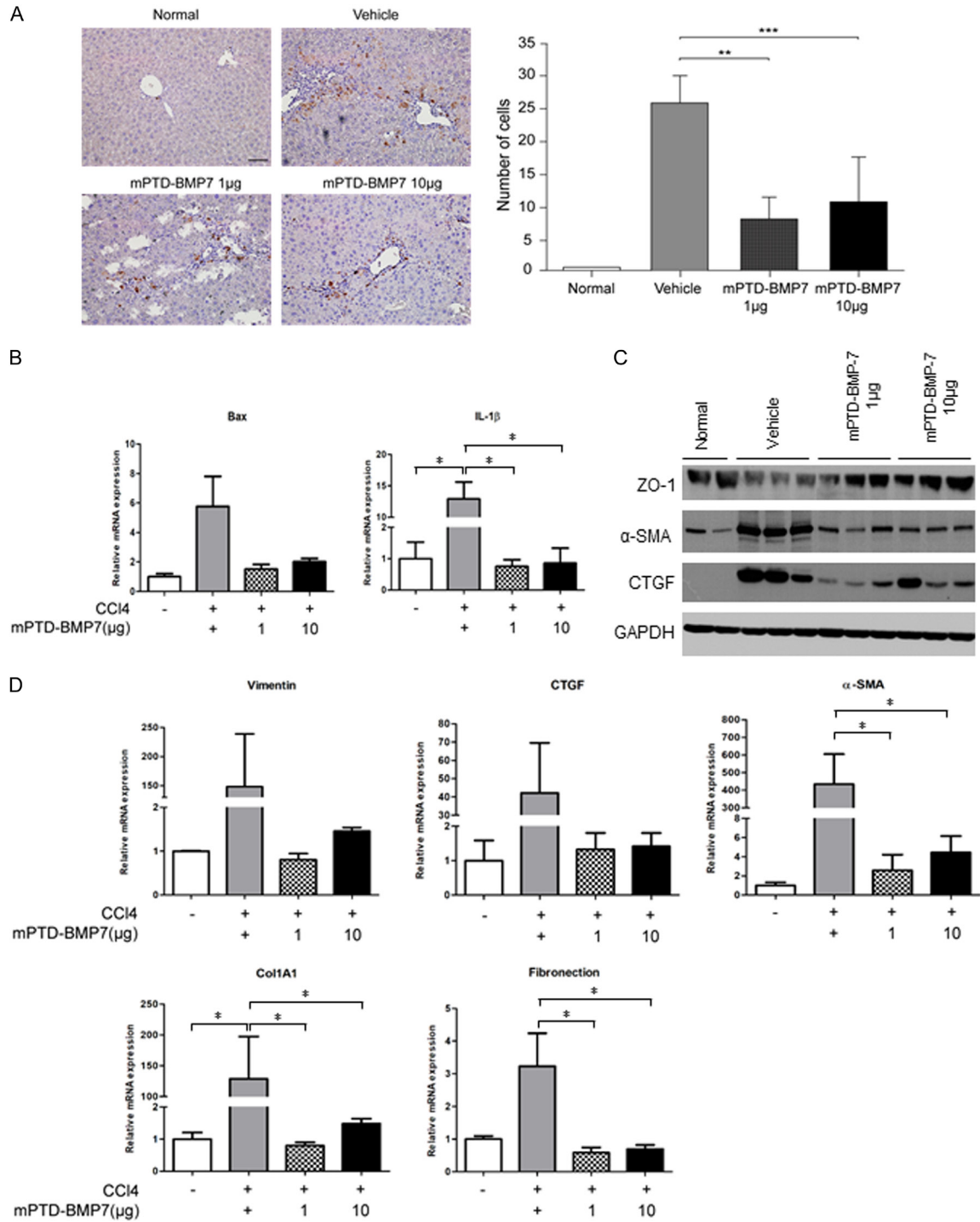


Figure 6. Effects on apoptosis, fibrogenic signaling, and EMT. A. Immunohistochemical staining for cleaved caspase-3 on paraffin sections from mice treated with vehicle, CCl₄, or CCl₄ + mPTD-BMP-7 for 12 weeks. Graph represents percentages of cleaved caspase-3-positive nuclei in tissues from each group (left). Quantitative analysis of cleaved caspase-3-positive hepatocytes in the indicated groups. Data are mean ± standard deviation of cleaved caspase-3-positive hepatocytes in a high-powered field (original magnification, 400×) (right). B. Quantitative real-time PCR assessment of the expression levels of the indicated genes in each group. C. Expression levels of the indicated genes were assessed by immunoblotting analysis of whole liver extracts. D. Quantitative real-time PCR assessment of the expression levels of fibrogenic and EMT genes. Data are presented as mean ± standard error of the mean (n=5).

Discussion

An association between the TGF- β signaling pathway and liver fibrosis has been demonstrated in fibrotic human livers and various animal models of liver fibrosis [30-32]. That local TGF- β activity has a substantial effect on liver fibrosis is evidenced by the fact that depletion of TGF- β in platelets attenuates CCl₄-induced liver fibrosis [33]. Thus, we hypothesized that BMP-7, which antagonizes TGF- β signaling in cells [21] and can reverse EMT during chronic renal fibrosis [9], might be similarly beneficial for preventing the progression of liver fibrosis. We found that, in HSCs, BMP-7 blocked TGF- β -dependent fibrogenic actions, thereby regulating the secretion of collagen and CTGF. Histopathological and biochemical analyses of hepatic tissue from CCl₄-induced liver fibrosis model mice confirmed distinct increases in liver enzyme levels in association with the increased expression levels of CTGF and α -SMA.

Although the physiological mechanism by which BMP-7 suppresses the TGF- β signaling pathway has been known for two decades, the current form of soluble recombinant human BMP-7 is minimally useful in a clinical setting because of its pharmacological limitations, such as rapid clearance and enzymatic degradation. To overcome the pharmacodynamic limitations of recombinant human BMP-7, we designed mPTD-BMP-7, with unique biological and pharmacological features. First, mPTD-BMP-7 is a prodrug that is transduced into cells and undergoes activation by endosomal machinery components including HSPs and furin endopeptidase, initiating BMP signal transduction. By contrast, current recombinant human BMPs directly target extracellular domains of BMPs. Second, mPTD-BMP-7 contains a prodomain for long-range action of latent BMP-7, whereas recombinant human BMP-7 consists only of active dimers. Although the prodomain of the TGF- β superfamily is largely ignored, it is required for binding to the extracellular matrix, which enables long-range action in vivo [34]. Moreover, latent TGF- β and BMP-7 sufficiently activate their signaling pathways without release of a prodomain from the latent complex [35, 36]. Third, we prepared the prodrug BMP-7 in a micelle nanocarrier to maximize delivery to the liver through intrave-

nous administration. We found that, following its initial burst release and rapid clearance [15], mPTD-BMP-7 exerted inhibitory effects on the pathogenesis of liver fibrosis. It also attenuated upregulation of α -SMA and CTGF and related histological changes induced by CCl₄ exposure, and protected tight junctions between hepatocytes.

Our study has several important clinical implications. First, a number of studies have shown that targeting TGF- β signaling may be a novel therapeutic strategy for the treatment of liver fibrosis, reflecting the role of TGF- β signaling in inflammation and fibrosis [37]. However, this strategy might also increase the risk of inflammation by blocking the anti-inflammatory properties of TGF- β . In addition, BMP-7 expression is very limited in adults, where it regulates multiple cellular processes, including cell differentiation and apoptosis in urinary-reproductive and gastrointestinal systems [38]. Because of its physiological abundance, BMP-7 is less toxic than other TGF- β inhibitors and can easily be applied in clinical treatment.

Second, fibrosis was at least partially TGF- β -dependent, implying that BMP-7 antagonizes the profibrogenic action of TGF- β in the liver. Disruption of the basement membrane with an abundant collagenous domain induced transition to a mesenchymal phenotype in the CCl₄-induced fibrosis group, which manifested as overexpression of α -SMA and fibronectin. Consistent with this finding, BMP-7 directly affected mRNA and protein expression levels of collagen 1; moreover, immunoblotting revealed lower levels of collagen in livers from mice treated with mPTD-BMP-7 than in control livers. Our results showed that mPTD-BMP-7 induced a dose-dependent reduction in CTGF expression through suppression of TGF- β by mPTD-BMP-7, which was upregulated by TGF- β activation. These findings strongly suggest that BMP-7 might serve as a suppressor of fibrosis in livers experiencing TGF- β -stimulated extracellular matrix degradation and HSC activation.

Third, BMP-7 is known to antagonize EMT during tissue repair, thereby alleviating the central component of cell-cell adhesion junctions, as demonstrated by the expression of E-cadherin and ZO-1 [39, 40]. In the context of fibrogenesis, dedifferentiation of epithelial cells

induces a mesenchymal-like phenotype and also causes downregulation of epithelial genes and upregulation of mesenchymal genes, all of which lead to the development of abnormal liver architecture and fibrotic septa. Our finding that mPTD-BMP-7 treatment was associated with restoration of ZO-1 and E-cadherin expression in livers implies that the tight junctions of hepatocytes play an essential role in the blood-biliary barrier. Notably, diminished tight junction expression has been observed in many cancers, and is closely associated with patient prognosis [41, 42]. These results strongly suggest that TGF- β -induced epithelial-myofibroblast transdifferentiation is regulated by BMP-7.

Fourth, serum ALT and AST levels, which have been used in the diagnosis of liver fibrosis, were positively correlated with liver injury and fibrosis [43]. The present study showed that the levels of serum AST and ALT, as well as the expression levels of pro-inflammatory mediators- such as IL-1 β -a potent pro-inflammatory mediator that exacerbates parenchymal cell injury [44] were significantly lower in mPTD-BMP-7-treated mice than in CCl₄ injured mice, suggesting that the active form of BMP-7 contributed to reduced vulnerability to CCl₄-induced liver fibrosis. The moderate reduction in hepatocyte death and parenchymal cell injury may be blocked by acute hepatic necroinflammation, while the progression of fibrosis is prevented by the antifibrogenic effects of BMP-7.

We acknowledge several limitations of this study. First, we presumed that BMP-7 negatively regulates the expression of TGF- β in liver fibrosis lesions. However, this inhibition manifests within a certain dose range; thus, BMP-7 might not antagonize TGF- β signaling in fibrogenesis in a dose-dependent manner. Second, our data demonstrated the anti-fibrogenic effect of BMP-7 only from a preventive point of view. An assessment of mPTD-BMP-7 as a next-generation growth factor therapy would require supplementing these findings with analyses of therapeutic effects in a liver fibrosis model. Although we attempted to systemically investigate the anti-fibrosis effects of mPTD-BMP-7, these studies lacked a clinical component. Addressing the above limitations will require further investigations of the regulatory mechanisms involving TGF- β and BMP-7 during the progression from fibrosis to cirrhosis-inves-

tigations that we plan to conduct in a future study.

Conclusions

In conclusion, our study showed that administration of mPTD-BMP-7 suppressed HSC activation and extracellular matrix accumulation in cultured LX2 cells, and in a mouse model of CCl₄-induced liver fibrosis. Collectively, our data demonstrate that mPTD-BMP-7, a prodrug of BMP-7, ameliorates liver fibrosis in this mouse model by suppressing the TGF- β signaling pathway.

Acknowledgements

This work was supported by grant from the Dongwha Faculty Research Assistance Program of Yonsei University College of Medicine (6-2019-0120), a grants from the National Research Foundation of Korea (NRF-2016R1E1A1A01942724, NRF-2017R1A2B3-002241, NRF-2019R1A2C2084535) funded by the Korea government (MSIP).

Disclosure of conflict of interest

J.I.Y. is an inventor of the patent related to this work filed by MET Life Sciences Co., Ltd. (Korean Patent Application Number: 10-2019-0076443, PCT Application Number: PCT/KR2020/007011). N.H.K., H.S.K., and J.I.Y. are the founders of MET Life Sciences Co., Ltd. and shareholder. All other authors declare that they have no competing interests.

Abbreviations

HSC, hepatic stellate cell; SMA, smooth muscle actin; TGF- β , transforming growth factor- β ; BMP, bone morphogenetic protein; EMT, epithelial-mesenchymal transition; PTD, protein transduction domain; CTGF, connective tissue growth factor; CCl₄, carbon tetrachloride; PCR, polymerase chain reaction.

Address correspondence to: Dr. Jong In Yook, Department of Oral Pathology, Oral Cancer Research Institute, Yonsei University College of Dentistry, 50-1 Yonsei-ro, Seodaemun-gu, Seoul, Korea. Tel: +82-2-2228-3032; Fax: +82-2-2228-3032; E-mail: JIYOOK@yuhs.ac; Dr. Seung Up Kim, Department of Internal Medicine, Yonsei University College of Medicine, 50-1 Yonsei-ro, Seodaemun-gu, Seoul, Korea. Tel: +82-2-2228-1944; Fax: +82-2-362-6884; E-mail: KSUKOREA@yuhs.ac

References

- [1] Herrera J, Henke CA and Bitterman PB. Extracellular matrix as a driver of progressive fibrosis. *J Clin Invest* 2018; 128: 45-53.
- [2] Yang JD. Detect or not to detect very early stage hepatocellular carcinoma? The western perspective. *Clin Mol Hepatol* 2019; 25: 335-343.
- [3] Hanouneh IA, Alkhouri N and Singal AG. Hepatocellular carcinoma surveillance in the 21st century: saving lives or causing harm? *Clin Mol Hepatol* 2019; 25: 264-269.
- [4] Ahn KS and Kang KJ. Appropriate treatment modality for solitary small hepatocellular carcinoma: radiofrequency ablation vs. resection vs. transplantation? *Clin Mol Hepatol* 2019; 25: 354-359.
- [5] Cai X, Li Z, Zhang Q, Qu Y, Xu M, Wan X and Lu L. CXCL6-EGFR-induced Kupffer cells secrete TGF-beta1 promoting hepatic stellate cell activation via the SMAD2/BRD4/C-MYC/EZH2 pathway in liver fibrosis. *J Cell Mol Med* 2018; 22: 5050-5061.
- [6] Dewidar B, Meyer C, Dooley S and Meindl-Beinker AN. TGF-beta in hepatic stellate cell activation and liver fibrogenesis-updated 2019. *Cells* 2019; 8: 1419.
- [7] Zhou L, Dong X, Wang L, Shan L, Li T, Xu W, Ding Y, Lai M, Lin X, Dai M, Bai X, Jia C and Zheng H. Casticin attenuates liver fibrosis and hepatic stellate cell activation by blocking TGF-beta/Smad signaling pathway. *Oncotarget* 2017; 8: 56267-56280.
- [8] Robert S, Gicquel T, Bodin A, Lagente V and Boichot E. Characterization of the MMP/TIMP imbalance and collagen production induced by IL-1beta or TNF-alpha release from human hepatic stellate cells. *PLoS One* 2016; 11: e0153118.
- [9] Zeisberg M, Hanai J, Sugimoto H, Mammoto T, Charytan D, Strutz F and Kalluri R. BMP-7 counteracts TGF-beta1-induced epithelial-to-mesenchymal transition and reverses chronic renal injury. *Nat Med* 2003; 9: 964-968.
- [10] Nishinakamura R and Sakaguchi M. BMP signaling and its modifiers in kidney development. *Pediatr Nephrol* 2014; 29: 681-686.
- [11] Shen B, Liu X, Fan Y and Qiu J. Macrophages regulate renal fibrosis through modulating TGFbeta superfamily signaling. *Inflammation* 2014; 37: 2076-2084.
- [12] Kinoshita K, Iimuro Y, Otogawa K, Saika S, Inagaki Y, Nakajima Y, Kawada N, Fujimoto J, Friedman SL and Ikeda K. Adenovirus-mediated expression of BMP-7 suppresses the development of liver fibrosis in rats. *Gut* 2007; 56: 706-714.
- [13] Hao ZM, Cai M, Lv YF, Huang YH and Li HH. Oral administration of recombinant adeno-associated virus-mediated bone morphogenetic protein-7 suppresses CCl(4)-induced hepatic fibrosis in mice. *Mol Ther* 2012; 20: 2043-2051.
- [14] Carreira AC, Zambuzzi WF, Rossi MC, Astorino Filho R, Sogayar MC and Granjeiro JM. Bone morphogenetic proteins: promising molecules for bone healing, bioengineering, and regenerative medicine. *Vitam Horm* 2015; 99: 293-322.
- [15] Kim NH, Cha YH, Kim HS, Lee SE, Huh JK, Kim JK, Kim JM, Ryu JK, Kim HJ, Lee Y, Lee SY, Noh I, Li XY, Weiss SJ, Jahng TA and Yook JI. A platform technique for growth factor delivery with novel mode of action. *Biomaterials* 2014; 35: 9888-9896.
- [16] Kabouridis PS. Biological applications of protein transduction technology. *Trends Biotechnol* 2003; 21: 498-503.
- [17] Lönn P, Kacsinta AD, Cui XS, Hamil AS, Kaulich M, Gogoi K and Dowdy SF. Enhancing endosomal escape for intracellular delivery of macromolecular biologic therapeutics. *Sci Rep* 2016; 6: 32301.
- [18] Song Y, Kim SH, Kim KM, Choi EK, Kim J and Seo HR. Activated hepatic stellate cells play pivotal roles in hepatocellular carcinoma cell chemoresistance and migration in multicellular tumor spheroids. *Sci Rep* 2016; 6: 36750.
- [19] Chung SI, Moon H, Kim DY, Cho KJ, Ju HL, Kim DY, Ahn SH, Han KH and Ro SW. Development of a transgenic mouse model of hepatocellular carcinoma with a liver fibrosis background. *BMC Gastroenterol* 2016; 16: 13.
- [20] Ishak K, Baptista A, Bianchi L, Callea F, De Groote J, Gudat F, Denk H, Desmet V, Korb G, MacSween RN and et al. Histological grading and staging of chronic hepatitis. *J Hepatol* 1995; 22: 696-699.
- [21] Boon MR, van der Horst G, van der Pluijm G, Tamsma JT, Smit JW and Rensen PC. Bone morphogenetic protein 7: a broad-spectrum growth factor with multiple target therapeutic potency. *Cytokine Growth Factor Rev* 2011; 22: 221-229.
- [22] Bach DH, Park HJ and Lee SK. The dual role of bone morphogenetic proteins in cancer. *Mol Ther Oncolytics* 2018; 8: 1-13.
- [23] Fog CK, Zago P, Malini E, Solanko LM, Peruzzo P, Bornaes C, Magnoni R, Mehmedbasic A, Petersen NHT, Bembi B, Aerts J, Dardis A and Kirkegaard T. The heat shock protein amplifier arimocloamol improves refolding, maturation and lysosomal activity of glucocerebrosidase. *EBioMedicine* 2018; 38: 142-153.
- [24] Xu J, Lamouille S and Derynck R. TGF-beta-induced epithelial to mesenchymal transition. *Cell Res* 2009; 19: 156-172.
- [25] Szeto SG, Narimatsu M, Lu M, He X, Sidiqi AM, Tolosa MF, Chan L, De Freitas K, Bialik JF, Ma-

- jumder S, Boo S, Hinz B, Dan Q, Advani A, John R, Wrana JL, Kapus A and Yuen DA. YAP/TAZ are mechanoregulators of TGF- β -Smad signaling and renal fibrogenesis. *J Am Soc Nephrol* 2016; 27: 3117-3128.
- [26] Liu Y, Liu H, Meyer C, Li J, Nadalin S, Königsrainer A, Weng H, Dooley S and ten Dijke P. Transforming growth factor- β (TGF- β)-mediated connective tissue growth factor (CTGF) expression in hepatic stellate cells requires Stat3 signaling activation. *J Biol Chem* 2013; 288: 30708-30719.
- [27] Lee Y, Kim NH, Cho ES, Yang JH, Cha YH, Kang HE, Yun JS, Cho SB, Lee SH, Paclikova P, Radzaskiewicz TW, Bryja V, Kang CG, Yuk YS, Cha SY, Kim SY, Kim HS and Yook JI. Dishevelled has a YAP nuclear export function in a tumor suppressor context-dependent manner. *Nat Commun* 2018; 9: 2301.
- [28] Tavares AJ, Poon W, Zhang YN, Dai Q, Besla R, Ding D, Ouyang B, Li A, Chen J, Zheng G, Robbins C and Chan WCW. Effect of removing Kupffer cells on nanoparticle tumor delivery. *Proc Natl Acad Sci U S A* 2017; 114: E10871-E10880.
- [29] Navarro-Corcuera A, Ansorena E, Montiel-Duarte C and Iraburu MJ. AGAP2: modulating TGFbeta1-signaling in the regulation of liver fibrosis. *Int J Mol Sci* 2020; 21: 1400.
- [30] Fabregat I, Moreno-Caceres J, Sanchez A, Dooley S, Dewidar B, Giannelli G and Ten Dijke P; IT-LIVER Consortium. TGF-beta signalling and liver disease. *FEBS J* 2016; 283: 2219-2232.
- [31] Xu Y, Sun X, Zhang R, Cao T, Cai SY, Boyer JL, Zhang X, Li D and Huang Y. A positive feedback loop of TET3 and TGF-beta1 promotes liver fibrosis. *Cell Rep* 2020; 30: 1310-1318, e1315.
- [32] Chung SI, Moon H, Ju HL, Cho KJ, Kim DY, Han KH, Eun JW, Nam SW, Ribback S, Dombrowski F, Calvisi DF and Ro SW. Hepatic expression of Sonic Hedgehog induces liver fibrosis and promotes hepatocarcinogenesis in a transgenic mouse model. *J Hepatol* 2016; 64: 618-627.
- [33] Ghafoory S, Varshney R, Robison T, Kouzbari K, Woolington S, Murphy B, Xia L and Ahamed J. Platelet TGF-beta1 deficiency decreases liver fibrosis in a mouse model of liver injury. *Blood Adv* 2018; 2: 470-480.
- [34] Gregory KE, Ono RN, Charbonneau NL, Kuo CL, Keene DR, Bächinger HP and Sakai LY. The prodomain of BMP-7 targets the BMP-7 complex to the extracellular matrix. *J Biol Chem* 2005; 280: 27970-27980.
- [35] Sengle G, Ono RN, Lyons KM, Bächinger HP and Sakai LY. A new model for growth factor activation: type II receptors compete with the prodomain for BMP-7. *J Mol Biol* 2008; 381: 1025-1039.
- [36] Campbell MG, Cormier A, Ito S, Seed RI, Bondesson AJ, Lou J, Marks JD, Baron JL, Cheng Y and Nishimura SL. Cryo-EM reveals integrin-mediated TGF- β activation without release from latent TGF- β . *Cell* 2020; 180: 490-501, e416.
- [37] Lan HY and Chung AC. TGF- β /Smad signaling in kidney disease. *Semin Nephrol* 2012; 32: 236-243.
- [38] Simon M, Maresh JG, Harris SE, Hernandez JD, Arar M, Olson MS and Abboud HE. Expression of bone morphogenetic protein-7 mRNA in normal and ischemic adult rat kidney. *Am J Physiol* 1999; 276: F382-389.
- [39] Kowanetz M, Valcourt U, Bergstrom R, Heldin CH and Moustakas A. Id2 and Id3 define the potency of cell proliferation and differentiation responses to transforming growth factor beta and bone morphogenetic protein. *Mol Cell Biol* 2004; 24: 4241-4254.
- [40] Zhang Q, Chang X, Wang H, Liu Y, Wang X, Wu M, Zhan H, Li S and Sun Y. TGF-beta1 mediated Smad signaling pathway and EMT in hepatic fibrosis induced by Nano NiO in vivo and in vitro. *Environ Toxicol* 2020; 35: 419-429.
- [41] Martin TA and Jiang WG. Loss of tight junction barrier function and its role in cancer metastasis. *Biochim Biophys Acta* 2009; 1788: 872-891.
- [42] Lee NP and Luk JM. Hepatic tight junctions: from viral entry to cancer metastasis. *World J Gastroenterol* 2010; 16: 289-295.
- [43] Zhang D, Hao X, Xu L, Cui J, Xue L and Tian Z. Intestinal flora imbalance promotes alcohol-induced liver fibrosis by the TGFbeta/smad signaling pathway in mice. *Oncol Lett* 2017; 14: 4511-4516.
- [44] Chen J, Hartono JR, John R, Bennett M, Zhou XJ, Wang Y, Wu Q, Winterberg PD, Nagami GT and Lu CY. Early interleukin 6 production by leukocytes during ischemic acute kidney injury is regulated by TLR4. *Kidney Int* 2011; 80: 504-515.